Heliyon 9 (2023) e19412

Contents lists available at ScienceDirect

Heliyon

journal homepage: www.cell.com/heliyon

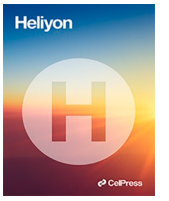

Hollow-core pear-shaped conjoined-tube fiber with low loss in the ultraviolet band

Yu Cheng [a,b,1], Yu Pan [a,b,1], Houquan Liu [a,b,*], Yiming Xiao [a,b], ShiJie Deng [a,b], Chuanxin Teng [a,b], Hongyan Yang [a,b], Hongchang Deng [a,b], Libo Yuan [a,b]

[a] School of Optoelectronic Engineering, Guilin University of Electronic Technology, Guilin, 541004, China
[b] Guangxi Key Laboratory of Optoelectronic Information Processing, Guilin University of Electronic Technology, Guilin, 541004, China

ARTICLE INFO

Keywords:
Hollow-core fiber
Pear-shaped tube
Ultraviolet band

ABSTRACT

PCTF (pear-shaped conjoined-tube fiber) is presented as a new ultraviolet (UV) guiding fiber with low loss. Results indicate that two PCTFs have better properties than that of previous studies in the UV band. The total loss of two PCTFs is less than 1 dB/km, and its bandwidth exceeds 150 nm between 0.2 and 0.4 μm. Furthermore, PCTF's single-mode performance is very promising, as evidenced by the higher-order mode extinction ratio (HOMER) over 10^3. The fabrication tolerance is discussed in this paper and results show that the tolerance is good enough to fabricate by normal fiber drawing process. This fiber is promising in applications for nonlinear optics, ultrafast optics, high power laser, and quantum optics.

1. Introduction

Hollow-core fibers (HCFs) with low loss are widely used in nonlinear optics, ultrafast optics, high power laser, and quantum optics [1–5]. In the past two decades, HCFs using various structure have been extensively studied due to their low loss properties and their ability to transmit in the terahertz, infrared, visible, and ultraviolet (UV) bands [6–9]. In a HCF, light is constrained in the air, so that material color centers are ignored, resulting in lower losses [10–12]. With the development of fiber drawing technology, microstructures have been adopted to improve the performance of optical fibers. Various structures are employed in HCFs to reduce loss. The main HCF structures are the photonic bandgap fiber (PBGF), the Kagome, the hollow-core anti-resonant fiber (ARF), the hollow-core nested anti-resonant nodeless fiber (NANF), and the conjoined-tube fiber (CTF) [6,13–16]. Recent studies have shown that NANF and CTF are most promising candidates to achieve ultra-low loss with large bandwidths in the terahertz, infrared, and visible wavelength ranges [16–24]. In 2018, a CTF with a minimal loss of 2 dB/km at 1512 nm was demonstrated by Shou-fei et al. [16]. Meanwhile, a NANF with an effective loss of 0.05 dB/m at 1 THz was reported by Hasanuzzaman et al. [22]. In 2020, a NANF with a minimum loss of 0.28 dB/km from 1510 to 1600 nm was reported by Jasion et al. In the same year, a NANF with an optical attenuation of 2.8 dB/km at 650 nm and 680 nm was reported by Sakr et al. [24]. In 2021, a NANF with a low loss of 0.22 dB/km at 1625 nm was reported by Sakr et al. [20]. In 2022, a NANF with double nested rings, namely DNANF, with a loss of 0.174 dB/km in the O-band was reported by Jasion et al. [21]. It is expected that the loss limit for conventional standard single-mode fibers (SSMFs) will soon be broken as this performance metric continues to decrease rapidly.

* Corresponding author. School of Optoelectronic Engineering, Guilin University of Electronic Technology, Guilin, 541004, China.
E-mail address: liuhouq@guet.edu.cn (H. Liu).
[1] These authors contribute equal to this work.

https://doi.org/10.1016/j.heliyon.2023.e19412
Received 28 February 2023; Received in revised form 6 July 2023; Accepted 22 August 2023
Available online 23 August 2023

In UV band, Février et al. first demonstrated the potential of HCF for UV transmission by measuring attenuation of 2 dB/m at 355 nm in 2009 [9]. Then, Yu et al. reported a ARF with attenuation of 0.08 dB/m and 0.26 dB/m at 218 nm and 355 nm, respectively in 2017 [25]. In most recent work on UV HCFs, Osório et al. reported a method to reduce the inner surface roughness of HCFs by improving the preparation process [26]. Their method can achieve a reduction in the root-mean-square of surface roughness from 0.40 nm to 0.15 nm, reducing the loss figure as low as 9.7 dB/km at 369 nm [26]. Chafer et al. reported two types of Raman laser sources that emit in the near-UV and mid-UV range using a heliostatic elastic gas-filled suppression-coupled HCF with low transmission loss (minimum 5 dB/km at 480 nm) [27]. And, Florian Leroi et al. reported a record of delivering high-energy signals in UV with a HCF. In their work, a 2 order of magnitude increase in fiber power handing in the UV range is achieved [28]. These works fully prove the potential of HCFs in UV band. In spite of this, in comparison to the excellent performance of HCF at other wavelength ranges, the potential of HCF in UV band has not yet been fully exploited. In this paper, two pear-shaped conjoined-tube fibers (PCTFs) in the UV band are proposed. The losses of the fibers, including surface scattering loss (SSL), the random micro-bend loss (RML) and confinement loss (CL) are analyzed. The total loss (CL + SSL + RML) of the two PCTFs is less than 1 dB/km at 300 nm, and its bandwidth exceeds 150 nm between 0.2 and 0.4 μm. In addition, the higher-order mode extinction ratio (HOMER) of PCTF-M has exceeded 10^3. There is evidence to suggest that the PCTF-M exhibits excellent single-mode characteristics. The proposed two fibers' tolerance is good enough to fabricate by normal fiber drawing process.

2. Structure and simulation

In Fig. 1(a) and (b), the cross sections of the two structures can be seen. In a pear-shaped conjoined tube structure, a short pear-shaped tube is embedded within a long pear-shaped tube. The two types of hollow-core pear-shaped conjoined-tube fiber (PCTF-M and PCTF-B) are classified according to the conjoined method (in Fig. 1(c)). The cross-section of the short pear-shaped tube of PCTF-M consists of two circular arcs of curvature R_1 and R_2 and two glass film of thickness t, the length of the short pear-shaped tube is d. The long pear-shaped tube of PCTF-M consists of two circular arcs of the same curvature R_3 and two glass film of thickness t. The length of the long pear-shaped tube is L. The connection between the long pear-shaped tube and the short pear-shaped tube is at the point where the length of the long pear-shaped tube $= (z + d\text{-}R_1)$, forming the middle pear-shaped conjoined tube (see Fig. 1(c)). The connection of PCTF-B is similar to PCTF-M, the difference is that the length L of the long pear-shaped tube of PCTF-B is shorter, and the short pear-shaped tube is connected to the bottom of the long pear-shaped tube. The structural parameters are listed in Table 1. The refractive index of glass is 1.45, and the air is 1.

In this study, COMSOL multiphysics based on the finite element method (FEM) is employed for numerical simulation. In order to obtain accurate simulation results, the maximum mesh sizes are selected as $\lambda/4$ for silica material region and adaptive mesh for air zone in the tubes (to maintain accuracy while reducing memory consumption), respectively [29,30]. A perfectly matched layer (PML) is placed outside the jacket layer to enclose the simulation area, to obtain the imaginary part of the mode eigenvalue to calculate the CL of fiber[29]. The thickness of the jacket layer and PML are set as 5 μm and 10 μm, respectively. The calculation formula of CL is expressed as follows [29,31,32]:

$$CL = 40\pi \times \mathrm{Im}(\mathrm{neff}) / [\ln(10) \times \lambda] \tag{1}$$

where, $\mathrm{Im}(\mathrm{neff})$ is the imaginary part of the effective refractive index, λ is the free space wavelength.

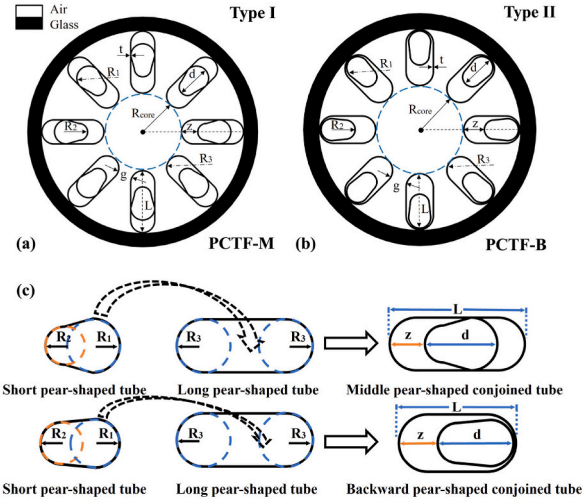

Fig. 1. The cross sections of two structures. (a) A middle hollow-core pear-shaped conjoined-tube fiber (PCTF-M). (b) A backward hollow-core pear-shaped conjoined-tube fiber (PCTF-B). (c) Composition of the backward pear-shaped conjoined tube and the middle pear-shaped conjoined tube (R_1, R_2 and R_3 are specially marked).

Table 1
The geometric parameters of the two PCTFs.

parameters	PCTF-M (μm)	PCTF-B (μm)	remarks
R_{core}	33	33	the core radius
R_1	10.88	8.88	the bottom radius
R_2	7.58	7.77	the top radius
R_3	10.88	10.88	the long tube radius
t	0.19	0.19	the glass thickness
g	13.48	13.48	the gap
z	13.98	14.10	the forward distance
d	29.53	29.22	the radial length
L	54.4	43.52	the long tube length

3. Results and discussion

3.1. Comparison of fiber structure in power density

There is an effective way to reduce CL. It is the structure of the cladding tube. Our fibers include PCTF-M and PCTF-B, which feature a pear-shaped conjoined tube structure that reduces CL effectively. Diagrams of the power density of four HCFs with the same core radius are shown in Fig. 2. The power density at the boundary (partly from −45° to 45°) shows clearly that the fiber's ability to constrain light. We compared the PCTF-M and PCTF-B with two HCFs, which were proposed by Ref. [15] and Ref. [33]. For data consistency, the core radius R_{core}, the capillary thickness t, and the tube gap g of the two PCTFs are kept the same in the comparison. The cross sections of HCFs are showed in Fig. 2(b), (c), 2(d) and 2(e) (red marks indicate calculated boundaries). According to Fig. 2(a), the two PCTFs have lower power density than NANF and ARF from −45° to 45°. And PCTF-B has the lowest power density. Thus, we conclude that the two pear-shaped conjoined-tube structures can effectively reduce the CL.

3.2. Comparison of fiber structure in CL

Firstly, we discuss how the structure of the cladding tube can decrease the CL (according to Eq. (1)). There are two methods that can be used to reduce CL. For the first one, a model of ideal HCF can be found in Ref. [18]. Silica and air have thicknesses of t and h, respectively. The ability of the ideal HCF to confine light can be characterized by Rm, and the Rm equal to $R_{core} + m\,(t + h)$. Using the theoretical formula of CL for the ideal HCF structure in Ref. [20] and Ref. [34], CL decreases rapidly as $(1/R_{core})^{2m+3}$. In this way, increasing m (the number of glass resonance layers) would be able to enhance the localization of light and reduce R_{core} or CL. And CL has an inverse correlation with $Rcore$. However, for realistic HCFs, CL~ $(1/R_{core})^{2m+3}$ is no longer valid and CL becomes proportional to $(1/R_{core})$ 4 for single-ring ARFs and $(1/R_{core})^8$ for NANFs [18]. The second method is based on increasing R_m to keep the core away from the nested point, which is the main leakage channel of NANFs [20]. This method has been mostly ignored before and was proposed recently [20]. In this paper, the R_m expressed as,

$$R_m = R_{\text{core}} + L \tag{2}$$

Therefore, the loss could be reduced by increasing Rm, namely, increase L. For verification, we compared PCTF-B, PCTF-M, ARF and NANF. The core radius R_{core}, the tube gap g and the capillary thickness t of these HCFs are fixed in Table 1. The cross sections and fundamental modes of the four HCFs are showed in Fig. 3(b)~(e). The PCTF-B and PCTF-M have lower CL than the other two HCFs in the range of 0.2~0.4 μm in Fig. 3(a). It is because the PCTF-B and PCTF-M have long pear-shaped tubes, which are much longer than

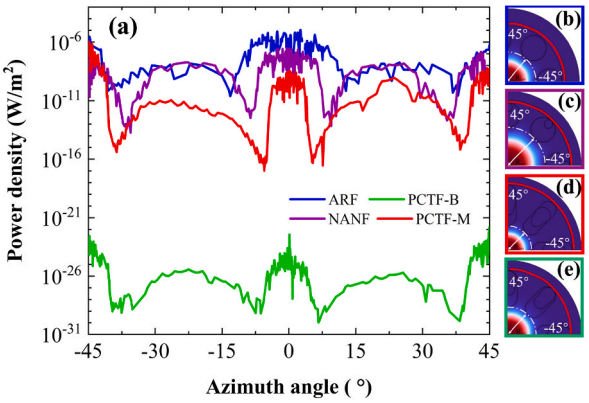

Fig. 2. (a) Power density distribution of ARF [33], NANF [15], PCTF-M and PCTF-B at the boundary. (b) The structure and the LP_{01} of ARF. (c) The structure and the LP_{01} of NANF. (d) The structure and the LP_{01} of PCTF-M. (e) The structure and the LP_{01} of PCTF-B.

the ARF and NANF's glass tubes. Thus, the R_m of PCTF-B and PCTF-M is much greater than that one of ARF and NANF. Therefore, we can conclude that PCTFs have better low-loss potential. The comparison between PCTF-B and PCTF-M shows that the CL level of PCTF-M is smaller than that of PCTF-B in the range of 0.2∼0.4 μm. Although PCTF-B has a smaller L than PCTF-M, it has a smaller CL than PCTF-M. It is caused by thick nodes forming at the intersection of the tubes of the middle pear-shaped conjoined tubes of PCTF-M (in Fig. 1(c)). Within the antiresonance window, these glass nodes cause additional resonance, which results in additional loss peaks and dips. Peaks and dips in the fiber can affect loss and dispersion characteristics and increase overall losses in the anti-resonant window [15]. By designing the fiber with the nodes as far away from the center as possible, the intensity of the loss level rise in the anti-resonant window can be reduced. For example, consider PCTF-B's design in Fig. 1(b). Therefore, PCTF-B can achieve lower loss by reducing the number of glass nodes in the pear-shaped tube to reduce its excess length L.

3.3. Fabrication tolerance

The two PCTFs have the characteristics of low CL and large bandwidth, but tolerance in optical fiber manufacturing is also key to practical application. To achieve better performance in the UV band, the two PCTFs have a thinner silicon film than most current HCFs. As a result, these two PCTFs cannot be drawn in any unusual way. A preform scale can be used to fabricate this PCTF with a target film thickness by minimizing pressure sensitivity by carefully designing the preforms. Using the drawing method proposed by Jackson et al. UV PCTF will be thinner [35]. And for the effect of surface roughness in the drawing process, Ref. [26] is used to reduce the roughness of the inner surface of the fiber during the drawing process to minimize the effect of SSL on the fiber performance. Geometric deviations are inevitable in the manufacture of HCFs. Initially, we consider that the deformation of the pear-shaped conjoined tube during the drawing process. The length of the long pear-shaped tube L changes directly as a result of this deformation. For greater clarity, we calculated the CL in Fig. 4(a) for L/R_1 at 1.0, 1.1, 1.9 and 2.7 in order to present a significant change in the long pear-shaped tube length L. The value of R_1 in L/R_1 has been fixed here in order to highlight the degree of deformation. In Fig. 4(a), the CL at $L/R_1 =$ 1.0 (red line) is at least two orders of magnitude higher than the CL at $L/R_1 = 2.7$ (black line) in the range of 0.2∼0.32 μm. In addition, the CL is decreasing in the range of 0.2∼0.4 μm as the L/R_1 ratio increases (the black arrow indicates a downward trend). The result ties well with the discussion in section 3.2. It indicates that the R_m increases with the length of the long pear-shaped conjoined tube L (as Eq. (2)). With an increase in R_m, HCF is likely to have a lower CL. Therefore, it can be concluded that the length of the long pear-shaped conjoined tube L is the most significant parameter in reducing CL. Secondly, we also consider that the impact of the positional error of the preform scale connection nodes on the CL performance of this fiber (PCTF-M). We analyze the impact of positional errors on the CL performance of the preform scale connection nodes. The CL is calculated in Fig. 4(b) for the four positions of the connection nodes (5 μm, 9 μm, 13 μm and 17 μm) in the range of 0.2∼0.4 μm. As can be seen in Fig. 4(b), the further away from the core the connection node is, the flatter CL will be (blue and red lines). As the connection node location approaches the core, the CL becomes less flat (e.g., black and green lines). In PCTF-M, location of the connected nodes affects CL. Further, we assume that imperfect pressure is also responsible for the deformation of the short pear-shaped tubes. A short pear-shaped tube collapsed into a circle is shown in Fig. 4(c)–(d) to demonstrate the impact of fabrication deformation on CL performance.

It shows the effect of top radius versus bottom radius from two PCTFs on CL as shown in Fig. 4(c)∼(d). It can be seen that if $\lambda =$ 0.255 μm, $R_2/R_1 = 0.71 \sim 0.91$, which can still maintain the same level of low-loss characteristics in the case of large differences in top and bottom radius. As a result, the bottom radius R_1 or top radius R_2 is not a key parameter for reducing CL. It can be concluded from the above discussion that structural deviation is influenced by three factors. A longer pear-shaped conjoined tube length L can reduce the level of CL. Then, the distance between the connecting node and the core of the pear-shaped conjoined tube can be increased to obtain a flatter CL curve. Finally, the top and bottom curvatures of a short pear-shaped tube have little effect on CL, so this factor can be ignored.

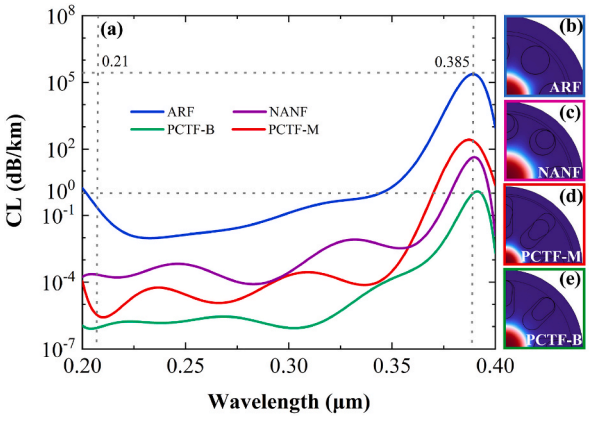

Fig. 3. (a) Diagrams of the CL of four HCFs. (b) The structure and LP_{01} of ARF[33]. (c) The structure and LP_{01} of NANF [15]. (d) The structure and LP_{01} of PCTF-M. (e) The structure and LP_{01} of PCTF-B.

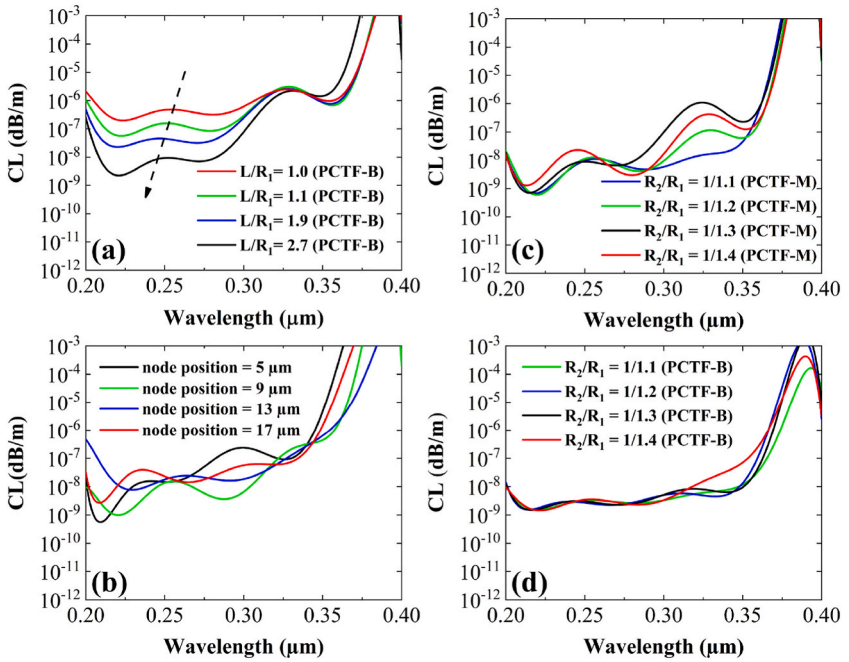

Fig. 4. (a) Diagram of CL of PCTF-B about the L/R_1 is 1.0, 1.1, 1.9, and 2.7, respectively. (b) Diagram of CL of PCTF-M about the node position is 5 μm, 9 μm, 13 μm, and 17 μm, respectively. (c) Diagram of CL of PCTF-M about the R_2/R_1 is 1/1.1, 1/1.2, 1/1.3, and 1/1.4, respectively. (d) Diagram of CL of PCTF-B about the R_2/R_1 is 1/1.1, 1/1.2, 1/1.3, and 1/1.4, respectively.

3.4. The higher-order mode extinction ratio

For HCF-based high power laser, the single-mode operation is one of the important requirements. This feature can be characterized by the loss ratio between the higher-order mode and the fundamental mode, also known as HOMER [18]. Fig. 5(b)–(c) showed the mode field distribution of LP_{01} mode and LP_{11} mode of PCTF-M. Fig. 5(a) showed the loss spectra of LP_{01} mode and LP_{11} mode, as well as the HOMER. We can see that in the range of 0.2~0.4 μm, the CL of LP_{11} mode as a whole was much larger than that of LP_{01} mode in the wavelength range of 0.34 μm. And the HOMER reached the maximum value of 10^3. So we can conclude that PCTF has excellent single-mode characteristics.

3.5. The SSL and the RML

In terms of overall losses, HCF is primarily affected by the CL, the RML and the SSL. In the previous section of the discussion, we have discussed the CL of PCTF. SSL and RML are discussed in this part. SSL is a loss caused by the surface roughness and the structure. It is inversely related to λ^3 [36]. And the SSL can be estimated after calibration [25,30,36–38],

$$SSL\left(dB/km\right) = \eta F(\lambda/\lambda_0)^{-3}\left(\mu m^{-1}\right) \tag{3}$$

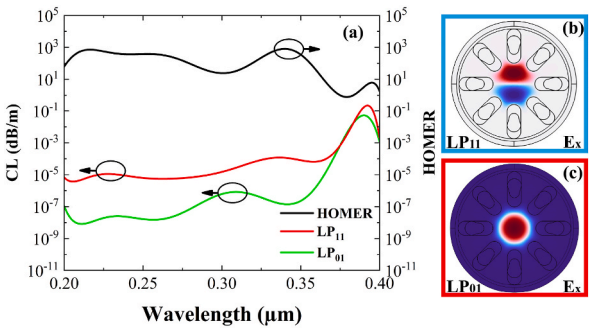

Fig. 5. (a) Diagram of CL of LP_{01} mode (green) and LP_{11} mode (red) from PCTF-M and the black line is HOMER. (b) The LP_{11} mode of PCTF-M (E_x). (c) The LP_{01} mode of PCTF-M (E_x).

$$F = \left(\frac{\varepsilon_0}{\mu_0}\right)^{\frac{1}{2}} \frac{\oint\limits_{\text{holeperimeters}} |E|^2 ds}{\iint\limits_{\text{cross-section}} E \times H^* dA} \tag{4}$$

where F is the power overlap between the fundamental mode and the silica boundary, and the calibration factor $\boldsymbol{\eta}$ is 300 when λ_0 is 1.55 μm [25,30,36–38]. Besides, the RML caused by the coupling between fundamental mode and LP_{11} mode can be calculated [30,32],

$$RML = \beta_0^2 C(\Delta\beta_{01}) \left(\langle 0|x^2|0\rangle - |\langle 0|x|1\rangle|^2 \right) \tag{5}$$

where $\boldsymbol{\beta}_0$ is the fundamental mode propagation constant and $\Delta\boldsymbol{\beta}_{01}$ is the difference of fundamental mode propagation constant and LP_{11} mode group propagation constant. C ($\Delta\boldsymbol{\beta}_{01}$) is the power spectral density at $\Delta\boldsymbol{\beta}_{01}$, $\langle 0|x|0\rangle$ and $\langle 0|x|1\rangle$ are the spot radius of fundamental mode and LP_{11} mode respectively [30,32].

For wavelengths less than 1 μm, the SSL starts to dominate, limiting the achievable loss in the visible range of the spectrum to ~10 dB/km [15]. However, the SSL can be effectively reduced by a better drawing process, which becomes urgent for the application of the HCF at short wavelengths [26]. To have a better understanding of the loss contributions of the SSL, we have done the theoretical analysis as shown in Fig. 6 (according to Eq. (3) and Eq. (4)). The SSL performances of the PCTF-M, the PCTF-B, the ARF and the NANF have been shown as the line with black, green, red and blue color respectively. And the SSL (black line) of the PCTF-M is almost equal to the one of the PCTF-B (green line). The SSL of the two PCTFs are lower in the short wavelength range (0.2~0.4 μm) than the ARF and the NANF. We also considered the effect of attenuation due to the RML, and we calculated the RML of PCTF-M and PCTF-B according to Eq. (5). Since the RML of PCTF-M and PCTF-B are close to each other, the gray dots in Fig. (6) represent the RML of the two fibers of PCTF. The results show that the RML is slightly higher than that of the SSL, and the RML has gradually become the primary cause of the attenuation in the short wavelength band (from 0.22 μm to 0.35 μm). Meanwhile, the losses (including the RML, the SSL and the CL) are lower than that of the NANF or the ARF, which resulted in the total loss of PCTF being lower than 1 dB/km in a wide wavelength range (from 0.2 μm to 0.4 μm). The essence of this phenomenon is the cross-section structure of the two PCTFs enables smaller mode overlap during fundamental mode transmission.

3.6. Comparison of loss with the proposed UV HCFs

In Table 2, we have compared the loss between our fibers and those from other typical reports. We are primarily comparing the five HCFs. It contains the core diameter, capillary thickness, and capillary diameter. It is noted that the HCFs reported in Ref. [26] and Ref. [27] have essentially the same parameters and that the fiber losses are close to each other. Secondly, after comparing the parameters of Ref. [39] and Ref. [25], the fibers obtained smaller losses when their capillary thicknesses were small under the condition of having close core diameters. There are large losses because the HCF has extra nodes as shown in Ref. [11]. Moreover, when comparing the HCFs of Ref. [11] and Ref. [26], we can conclude that larger core diameters reduce loss. In conclusion, low-loss fibers have a suitable core radius and a smaller capillary thickness. And our PCTFs simulate the lowest loss currently available in the UV band.

4. Conclusion

In this paper, we proposed two PCTFs (including PCTF-M and PCTF-B) with low transmission loss for UV waveguiding. The losses of the two PCTFs, including the SSL, the RML and the CL are discussed. The total loss of the two PCTFs is less than 1 dB/km at 300 nm, and its bandwidth exceeds 150 nm between 0.2 and 0.4 μm. In addition, the HOMER of PCTF-M has exceeded 10^3. There is evidence to suggest that the PCTF-M exhibits excellent single-mode characteristics. The proposed two fibers' tolerance is good enough to fabricate by normal fiber drawing process. In order to maintain low loss characteristics, the length of the long pear-shaped tube L should increase as allowed if the radius of the core R_{core} is fixed. According to the study results, the PCTF has potential applications in the areas of nonlinear optics, ultrafast optics, high power laser, and quantum optics.

Funding

The authors thank the National Natural Science Foundations of China (Nos. 62065006, 61975038, 62075047, 61965006, 61535004, 61735009, 61964005, 61805050, 61675052, and 61640409), Innovation Project of GUET Graduate Education (No. 2023YCXS201) for their support.

Author contribution statement

Yu Cheng, Yu Pan & Houquan Liu: Conceived and designed the experiments; Analyzed and interpreted the data; Wrote the paper. Yiming Xiao, ShiJie Deng, Chuanxin Teng, Hongyan Yang, Hongchang Deng & Libo Yuan: Analyzed and interpreted the data; Wrote the paper.

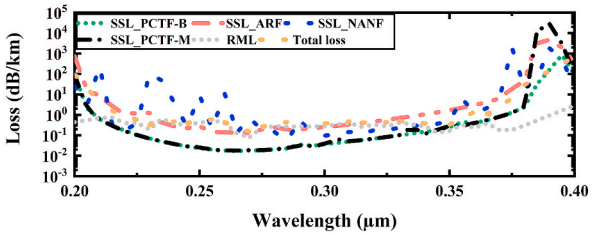

Fig. 6. Calculated the losses of ARF, NANF, PCTF-M and PCTF-B. Surface scattering loss (SSL) spectra for fibers in ARF, NANF, PCTF-M and PCTF-B. The gray dot-dashed line is the RML of the two PCTFs, almost identical to that of PCTF-M.

Table 2
Comparison of loss with proposed UV hollow-core fibers.

Ref.	Core dia. (μm)	Tube dia. (μm)	*t* (μm)	Loss (dB/km)
[26]	27	11	0.6	9.7 (369 nm)
[27]]	27	11	0.6	5 (480 nm)
[39]	14.6	20.87	0.615	300 (355 nm)
[11]	17.7	38	0.56	2400 (348 nm)
[25]	17	7.3	0.133	80 (218 nm)
Our work	66	43.52	0.19	<1 (300 nm)

Data availability statement

Data will be made available on request.

Additional information

No additional information is available for this paper.

Declaration of competing interest

The authors declare no conflicts of interest.

References

[1] P.S. Russell, P. Holzer, W. Chang, et al., Hollow-core photonic crystal fibres for gas-based nonlinear optics, Nat. Photonics 8 (4) (2014) 278–286.
[2] F. Couny, F. Benabid, P.J. Roberts, et al., Generation and photonic guidance of multi-octave optical-frequency combs, Science 318 (5853) (2007) 1118–1121.
[3] T. Balciunas, C. Fourcade-Dutin, G. Fan, et al., A strong-field driver in the single-cycle regime based on self-compression in a kagome fibre, Nat. Commun. 6 (2015).
[4] Y.Y. Wang, M. Alharbi, T.D. Bradley, et al., Hollow-core photonic crystal fibre for high power laser beam delivery, High Power Laser Science and Engineering 1 (1) (2013) 17–28.
[5] M.R. Sprague, P.S. Michelberger, T.F.M. Champion, et al., Broadband single-photon-level memory in a hollow-core photonic crystal fibre, Nat. Photonics 8 (4) (2014) 287–291.
[6] A.D. Pryamikov, A.S. Biriukov, A.F. Kosolapov, et al., Demonstration of a waveguide regime for a silica hollow-core microstructured optical fiber with a negative curvature of the core boundary in the spectral region > 3.5 μm, Opt Express 19 (2) (2011) 1441–1448.
[7] F. Yu, P. Song, D.K. Wu, et al., Attenuation limit of silica-based hollow-core fiber at mid-IR wavelengths, Apl Photonics 4 (8) (2019).
[8] M. Chafer, J.H. Osorio, F. Amrani, et al., 1-km hollow-core fiber with loss at the silica Rayleigh limit in the green spectral region, IEEE Photon. Technol. Lett. 31 (9) (2019) 685–688.
[9] S. Fevrier, F. Gerome, A. Labruyere, et al., Ultraviolet guiding hollow-core photonic crystal fiber, Opt Lett. 34 (19) (2009) 2888–2890.
[10] D.G. Ouzounov, F.R. Ahmad, D. Muller, et al., Generation of megawatt optical solitons in hollow-core photonic band-gap fibers, Science 301 (5640) (2003) 1702–1704.
[11] A. Hartung, J. Kobelke, A. Schwuchow, et al., Double antiresonant hollow core fiber - guidance in the deep ultraviolet by modified tunneling leaky modes, Opt Express 22 (16) (2014) 19131–19140.
[12] R.F. Cregan, B.J. Mangan, J.C. Knight, et al., Single-mode photonic band gap guidance of light in air, Science 285 (5433) (1999) 1537–1539.
[13] J.C. Knight, J. Broeng, T.A. Birks, et al., Photonic band cap guidance in optical fibers, Science 282 (5393) (1998) 1476–1478.
[14] M.K. Mridha, D. Novoa, P.S. Russell, Dominance of backward stimulated Raman scattering in gas-filled hollow-core photonic crystal fibers, Optica 5 (5) (2018) 570–576.
[15] F. Poletti, Nested antiresonant nodeless hollow core fiber, Opt Express 22 (2014).
[16] S.F. Gao, Y.Y. Wang, W. Ding, et al., Ultralow loss hollow-core conjoined-tube negative-curvature fiber, in: Conference on Fiber Lasers XVI - Technology and Systems, San Francisco, CA, 2019.
[17] W. Ding, Y.Y. Wang, S.F. Gao, et al., Recent progress in low-loss hollow-core anti-resonant fibers and their applications, IEEE J. Sel. Top. Quant. Electron. 26 (4) (2020).
[18] Y. Zhu, W. Li, F. Gao, et al., Small-core hollow-core nested antiresonant nodeless fiber with semi-circular tubes, Opt Express 30 (12) (2022) 20373–20388.
[19] L. Vincetti, Empirical formulas for calculating loss in hollow core tube lattice fibers, Opt Express 24 (10) (2016).
[20] H. Sakr, T.D. Bradley, G.T. Jasion, et al., Hollow core NANFs with five nested tubes and record low loss at 850, 1060, 1300 and 1625nm, in: Optical Fiber Communications Conference and Exhibition (OFC), Electr Network, 2021.

[21] G.T. Jasion, H. Sakr, J.R. Hayes, et al., 174 dB/km hollow core double nested antiresonant nodeless fiber (DNANF), in: Optical Fiber Communications Conference and Exhibition (OFC), San Diego, CA, 2022, 0.
[22] G.K.M. Hasanuzzaman, S. Iezekiel, C. Markos, et al., Hollow-core fiber with nested anti-resonant tubes for low-loss THz guidance, Opt Commun. 426 (2018) 477–482.
[23] G.T. Jasion, T.D. Bradley, K. Harrington, et al., Hollow core NANF with 0.28 dB/km attenuation in the C and L bands, in: Optical Fiber Communications Conference and Exposition (OFC), San Diego, CA, 2020.
[24] H. Sakr, Y. Chen, T. Bradley, et al., Advances in Hollow Core Fiber for the 1μm and Visible Wavelength Regions, 2020.
[25] F. Yu, W. Wadsworth, J. Knight, Low-Loss Silica Hollow-Core Fiber for UV, 2017. ATu5A.4.
[26] J.H. Osório, F. Amrani, F. Delahaye, et al., Hollow-core fibers with ultralow loss in the ultraviolet range and sub-thermodynamic equilibrium surface-roughness, in: 2022 Conference on Lasers and Electro-Optics, CLEO), 2022.
[27] M. Chafer, J.H. Osorio, A. Dhaybi, et al., Near- and middle-ultraviolet reconfigurable Raman source using a record-low UV/visible transmission loss inhibited-coupling hollow-core fiber, Opt Laser. Technol. 147 (2022).
[28] F. Leroi, F. Gérôme, J. Didierjean, et al., UV 20W-class single-mode nanosecond pulse delivery using a vacuum-free/ambient air inhibited-coupling hollow-core fiber, Applied Physics B 129 (2023).
[29] K.S.R. Shaha, A. Khaleque, M.S. Hosen, Wideband Low Loss Hollow Core Fiber With Nested Hybrid Cladding Elements, Journal of Lightwave Technology 39 (20) (2021) 6585–6591.
[30] W. Zheng, Y. Qin, O. Xu, et al., Wideband low confinement loss anti-resonant hollow core fiber with nested U-shape tube, Optics Express 29 (15) (2021) 24182–24192.
[31] T.P. White, B.T. Kuhlmey, R.C. McPhedran, et al., Multipole method for microstructured optical fibers. I. Formulation, J. Opt. Soc. Am. B 19 (10) (2002) 2322–2330.
[32] X. Chen, X. Hu, L. Yang, et al., Double negative curvature anti-resonance hollow core fiber, Opt Express 27 (14) (2019) 19548–19554.
[33] F. Yu, M. Cann, A. Brunton, et al., Single-mode solarization-free hollow-core fiber for ultraviolet pulse delivery, Opt Express 26 (8) (2018) 10879–10887.
[34] M.S. Habib, C. Markos, R. Amezcua-Correa, Impact of cladding elements on the loss performance of hollow-core anti-resonant fibers, Opt Express 29 (3) (2021) 3359–3374.
[35] G. Jackson, T. Bradley, G. Jasion, et al., Exploring Fabrication Limits for UV Guiding Hollow Core Anti-resonant Fiber, 2021. FW1C.3.
[36] P.J. Roberts, F. Couny, H. Sabert, et al., Ultimate low loss of hollow-core photonic crystal fibres, Opt Express 13 (1) (2005) 236–244.
[37] E.N. Fokoua, F. Poletti, D.J. Richardson, Analysis of light scattering from surface roughness in hollow-core photonic bandgap fibers, Opt Express 20 (19) (2012) 20980–20991.
[38] E. Fokoua, abokkhamis mousavi, G. Jasion, et al., Loss in hollow core optical fibers: mechanisms, scaling rules and limits, Advances in Optics and Photonics 15 (2022).
[39] Y. Wang, W. Ding, S. Gao, Hollow-core negative-curvature fiber for UV guidance, Optics Letters 43 (2018).